Int. J. Heat Mass Transfer. Vol. 35, No. 10, pp. 2389–2401, 1992
Printed in Great Britain

0017 9310/92 $5.00 + 0.00

Evaporation and growth dynamics of a layered droplet

V. BHARAT and ASIT K. RAY†
Department of Chemical Engineering, University of Kentucky, Lexington, KY 40506–0046, U.S.A.

(*Received* 18 *March* 1991 *and in final form* 5 *November* 1991)

Abstract—A mathematical model has been formulated for the evaporation and growth of a two-phase isolated droplet of two partially miscible components, exposed to a stagnant gas phase. Unsteady-state transport equations of the two components in the core, shell and gas phases have been rigorously treated. The resulting mathematical model involving two moving boundaries at the core–shell interface and the droplet–gas interface has been solved numerically for various conditions. Effects of critical parameters on the droplet dynamics have been examined. In a vapor free atmosphere where both components evaporate, the results show that the core either grows or evaporates depending on the physical parameters. When the core evaporates, either the shell or core disappears first, leaving a single-phase droplet. The study shows that the volatility of the components, thermodynamic and transport parameters greatly influence the evaporation behavior of a layered droplet.

1. INTRODUCTION

THE GROWTH or evaporation of multicomponent, multiphase droplets is a process of interest in the study of cloud formation, spray drying, droplet combustion and coating of agricultural spray. Although evaporation and growth of single phase droplets containing one or more components have been examined in numerous studies [1–6], only a few studies have been devoted to droplets containing immiscible or partially miscible components. Law *et al.* [7] have analyzed the combustion characteristics of water-in-oil emulsion droplets and indicated that the presence of water improves the combustion efficiency of hydrocarbon fuels. Avedisian and Fatehi [8] have also examined the evaporation characteristics of emulsified liquid droplets. For water–heptane emulsion droplets, they found that the slightly less volatile component, water, preferentially evaporated from the droplets. The coalescence of internal microdroplets in an unstable emulsified droplet results in the formation of either a core or a shell, thus leading to the creation of a layered droplet. Condensation of an immiscible phase on a homogeneous droplet can also produce a layered droplet. It has been demonstrated that compressed monolayers of insoluble surfactants forming rigid surface films provide high interfacial resistance to mass transfer [9–12]. The reduction in the transfer rate through such a surface film cannot be explained by the Fickian diffusion model [13]. It has also been observed that soluble or expanded surfactant films offer little or no interfacial resistance to mass transfer [14–16]. These studies indicate that the formation of rigid, immobile, somewhat ordered interfaces provide surface barriers to mass transfer, whereas expanded, liquid like mobile surface layers offer little or no barrier to mass transfer.

Despite its importance in many physical and industrial processes, the problem of evaporation and growth of layered droplets has not been examined theoretically up to this time. In the present study, we shall rigorously examine the dynamic behavior of a two-phase binary droplet, of partially miscible components, exposed to a stagnant gas phase. The partially miscible components form two distinct phases consisting of the core and shell of the droplet. The study is unique in the sense that it considers the movement of two phase boundaries at the core–shell interface and the droplet–gas interface, along with the concentration distributions in the core, shell and gas phases. A somewhat analogous problem involving bubble growth inside a droplet suspended in an immiscible liquid has been analyzed by Avedisian and Suresh [17]. In such a problem, the conservation of mass dictates a fixed relationship between the bubble radius and the outer radius of the droplet at all times. In the present problem no such relationship exists between the core and outer radii, and their changes are dictated by interfacial transfer rates. The model also considers core and shell phase convections generated by the density difference between the two components. Readey and Cooper [18] were the first to consider such convection in their analysis of dissolution or growth of a crystal from a non-zero initial size. Solutions of the model are accomplished by numerical methods, and are critically examined to determine the factors that affect evaporation and growth kinetics.

2. MODEL FORMULATION

A schematic view of the physical situation involved in the problem is shown in Fig. 1. A stationary coated droplet composed of two components A and B that

† Author to whom correspondence should be sent.

NOMENCLATURE

a	droplet radius
$\hat{a}_j^i$	$\gamma_j^i x_j^i$, activity of component j (= A, B) in phase i (= ′, ″)
A	dimensionless droplet radius
A_p	van Laar constant
b	$\bar{\rho}_B/\bar{\rho}_A$, ratio of pure component liquid phase densities
B_p	van Laar constant
C_j	gas phase concentration of component j (= A, B)
D_j	gas phase diffusion coefficient of component j (= A, B)
D_L^i	diffusion coefficient in the droplet phase i (= ′, ″)
$\mathscr{D}_j$	D_j/D_L', dimensionless gas phase diffusion coefficient of component j (= A, B)
$\mathscr{D}_L$	D_L''/D_L', dimensionless liquid phase diffusion coefficient
$f^i(t)$	arbitrary function of integration
m_j	total mass of component j (= A, B) in the droplet
M_j	molecular weight of component j (= A, B)
P_j°	vapor pressure of component j (= A, B)
r	radial position
R	universal gas constant
s_j	$C_{j\infty}/C_{je}$, saturation ratio of component j (= A, B) in bulk gas
t	time
T	temperature
v^i	convective velocity in the droplet phase i (= ′, ″)
V	droplet volume
w_j^i	weight fraction of component j (= A, B) in the droplet phase i (= ′, ″)
x_j^i	mole fraction of component j (= A, B) in the droplet phase i (= ′, ″)
X	dimensionless position defined by equation (32)
Y	dimensionless position defined by equation (33)
Z	dimensionless position defined by equation (34).

Greek symbols

β	P_B°/P_A°, relative volatility parameter
γ_j^i	activity coefficient of component j (= A, B) in the droplet phase i (= ′, ″)
ε	$C_{Ac}/\bar{\rho}_B$, volatility parameter
μ	M_A/M_B, ratio of molecular weights
ρ^i	total mass density of the droplet phase i (= ′, ″)
ρ_j^i	mass concentration of component j (= A, B) in the droplet phase i (= ′, ″)
$\bar{\rho}_j$	liquid phase density of pure component j (= A, B)
σ	effective infinity factor
τ	$D_L' t/a_i^2$, dimensionless time
ψ_j	dimensionless concentration of component j (= A, B).

Subscripts

A	component A
B	component B
c	core droplet
e	value at saturated state
i	initial value
j	component A or B
L	liquid phase
m	value at the miscibility limit composition $x_A^i = x_{Am}^i$
s	value at the droplet surface
∞	bulk gas.

Superscripts

i	core phase for i = ″, and shell phase i = ′
–	pure component
′	core phase.

are partially miscible is exposed to a stagnant gas phase containing A, B and a non-transferring species C. The partially miscible components form two distinct phases consisting of the core and shell of the droplet. Initially, the two phases (shell and core) are in equilibrium with one another, and their compositions are given by the miscibility limits. The droplet either evaporates or grows depending on the bulk gas phase composition. In the mathematical formulation of the problem we shall invoke the following assumptions.

(i) The droplet evaporates or grows relatively slowly, thus the system remains nearly isothermal.

(ii) The core droplet remains at the geometric center of the system at all times, and the outer phase exists in the form of a concentric shell surrounding the core droplet. Ray *et al.* [19] have experimentally observed that core and shell phases form concentric spheres in layered droplets except for tiny cores. In latter situations, the location of a tiny core droplet inside a large immiscible droplet has no effect on the mass transfer rate.

(iii) The densities of the two phases in the droplet change with composition. No volume change, however, occurs due to the mixing of the two components (ideal mixing). This assumption implies that the excess molar volume is negligible compared to the

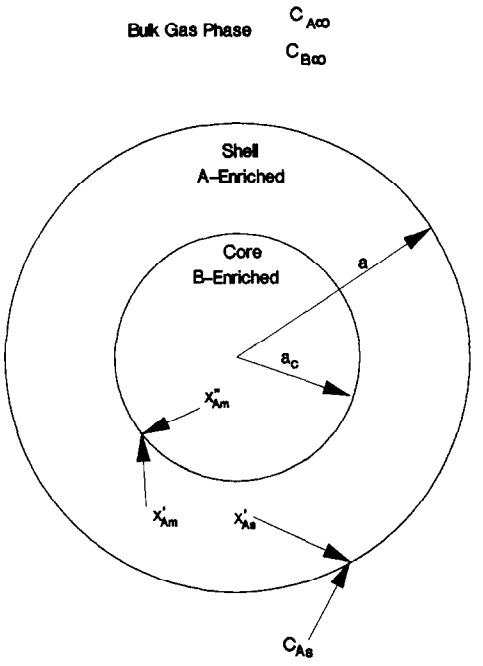

FIG. 1. A schematic description of the problem.

molar volumes of the individual components and this condition is satisfied if the mixing of the components does not result in the evolution or absorption of any significant amount of heat.

(iv) The saturation concentrations of A and B in the gas phase are negligibly small compared with the concentration of the non-transferring species. The density of the gas phase remains constant at all times, and the gas phase convection (Stefan flow) is neglected. The analyses of Rosner and Chang [20] and Huckaby and Ray [6] show that the gas phase convection can be neglected if $(\rho_v/\rho_g) \leqslant 0.10$, where ρ_v and ρ_g are the saturated vapor mass concentration and gas phase density, respectively.

(v) The gas–liquid and liquid–liquid interfaces of the system remain at equilibrium at all times. This assumption implies that there is no interfacial resistance to mass transfer.

(vi) The diffusion coefficients of A and B in the gas and liquid phases are independent of compositions.

With the above assumptions, the following partial differential equations govern the transfer of species A and B.

Core and shell phases

Species balance on A

$$\frac{\partial \rho^i_A}{\partial t} = \frac{1}{r^2}\frac{\partial}{\partial r}\left(r^2 \rho^i D^i_L \frac{\partial w^i_A}{\partial r}\right) - \frac{1}{r^2}\frac{\partial}{\partial r}(r^2 \rho^i_A v^i) \quad (1)$$

Continuity equation

$$\frac{\partial \rho^i}{\partial t} = -\frac{1}{r^2}\frac{\partial}{\partial r}(r^2 \rho^i v^i) \quad (2)$$

where superscript $i = '$ or $''$ denotes the shell or the core phase, respectively.

Gas phase

Species balance

$$\frac{\partial C_j}{\partial t} = \frac{1}{r^2}\frac{\partial}{\partial r}\left(r^2 D_j \frac{\partial C_j}{\partial r}\right) \quad (3)$$

where subscript $j = $ A or B stands for component A or B.

The following boundary and initial conditions apply to the above system of partial differential equations.

At $r = 0$

$$\rho'' D''_L \frac{\partial w''_A}{\partial r} - \rho''_A v'' = 0 \quad (4)$$

At the core–shell interface $(r = a_c)$

Equilibrium conditions

$$\gamma'_{jm} x'_{jm} = \gamma''_{jm} x''_{jm} \quad (5)$$

Species balance on A

$$\rho'_A \frac{da_c}{dt} + \rho' D'_L \frac{\partial w'_A}{\partial r} - \rho'_A v' = \rho''_A \frac{da_c}{dt} + \rho'' D''_L \frac{\partial w''_A}{\partial r} - \rho''_A v'' \quad (6)$$

At the gas–droplet interface $(r = a)$

Equilibrium conditions

$$C_j = \frac{\gamma'_j x'_j P^\circ_j M_j}{RT} \quad (7)$$

Species balance

$$D_j \frac{\partial C_j}{\partial r} + C_j \frac{da}{dt} = \rho'_j \frac{da}{dt} + \rho' D'_L \frac{\partial w'_j}{\partial r} - \rho'_j v' \quad (8)$$

Bulk gas phase $(r \to \infty)$

$$C_j = C_{j\infty} \quad (9)$$

Initial conditions $(t = 0)$

Core phase $(0 \leqslant r \leqslant a_c)$

$$w''_A = w''_{Am} \quad (10)$$

Shell phase $(a_c \leqslant r \leqslant a)$

$$w'_A = w'_{Am} \quad (11)$$

Gas phase $(a \leqslant r < \infty)$

$$C_j = C_{j\infty}. \quad (12)$$

To solve equations (1) and (2), describing the concentration profiles in the core and shell phases, we need to develop a relation between the velocity and composition. Since ρ^i and ρ^i_A are functions of w^i_A only, we may rewrite equations (1) and (2) in the

following forms

$$\left(\frac{\mathrm{d}\rho_{\mathrm{A}}^{i}}{\mathrm{d}w_{\mathrm{A}}^{i}}\right)\frac{\partial w_{\mathrm{A}}^{i}}{\partial t}=\frac{1}{r^{2}}\frac{\partial}{\partial r}\left(r^{2}\rho^{i}D_{\mathrm{L}}^{i}\frac{\partial w_{\mathrm{A}}^{i}}{\partial r}\right)-\frac{\rho_{\mathrm{A}}^{i}}{r^{2}}\frac{\partial}{\partial r}(r^{2}v^{i})-v^{i}\left(\frac{\mathrm{d}\rho_{\mathrm{A}}^{i}}{\mathrm{d}w_{\mathrm{A}}^{i}}\right)\frac{\partial w_{\mathrm{A}}^{i}}{\partial r}\quad(13)$$

and

$$\left(\frac{\mathrm{d}\rho^{i}}{\mathrm{d}w_{\mathrm{A}}^{i}}\right)\frac{\partial w_{\mathrm{A}}^{i}}{\partial t}=-\frac{\rho^{i}}{r^{2}}\frac{\partial}{\partial r}(r^{2}v^{i})-v^{i}\left(\frac{\mathrm{d}\rho^{i}}{\mathrm{d}w_{\mathrm{A}}^{i}}\right)\frac{\partial w_{\mathrm{A}}^{i}}{\partial r}\quad(14)$$

The following relations apply between the mass density ρ^{i}, mass concentration of A ρ_{A}^{i}, and weight fraction w_{A}^{i},

$$\frac{\rho_{\mathrm{A}}^{i}}{\rho^{i}}=w_{\mathrm{A}}^{i}\quad(15)$$

and

$$\rho^{i}\frac{\mathrm{d}\rho_{\mathrm{A}}^{i}}{\mathrm{d}w_{\mathrm{A}}^{i}}-\rho_{\mathrm{A}}^{i}\frac{\mathrm{d}\rho^{i}}{\mathrm{d}w_{\mathrm{A}}^{i}}=(\rho^{i})^{2}.\quad(16)$$

Eliminating the time derivatives from equations (13) and (14), and using equation (16), we obtain the following relation between the velocity and composition distributions:

$$\frac{\partial}{\partial r}(r^{2}v^{i})=-\frac{\mathrm{d}\rho^{i}}{\mathrm{d}w_{\mathrm{A}}^{i}}\frac{1}{(\rho^{i})^{2}}\frac{\partial}{\partial r}\left(r^{2}\rho^{i}D_{\mathrm{L}}^{i}\frac{\partial w_{\mathrm{A}}^{i}}{\partial r}\right).\quad(17)$$

To solve for the velocity profiles, we need a relation between the total mass density and weight fraction. In the present study, we invoke assumption (iii) (i.e. volume does not change due to mixing) which yields the following relation between the mass density and weight fraction

$$\rho^{i}=\frac{\bar{\rho}_{\mathrm{B}}}{1-(1-b)w_{\mathrm{A}}^{i}}\quad(18)$$

where $b=\bar{\rho}_{\mathrm{B}}/\bar{\rho}_{\mathrm{A}}$, and $\bar{\rho}_{\mathrm{A}}$ and $\bar{\rho}_{\mathrm{B}}$ are the pure component liquid phase mass densities of A and B, respectively. Integrating equation (17) with the use of equation (18), we obtain

$$r^{2}v^{i}=-r^{2}\frac{D_{\mathrm{L}}^{i}}{\rho^{i}}\frac{\partial\rho^{i}}{\partial r}+f^{i}(t)\quad(19)$$

where $f^{i}(t)$ is an arbitrary function of integration. Since the density and velocity must have finite values at the center of the droplet ($r=0$), the function of integration $f''(t)$, must be equal to zero for the core phase. The velocity in the core phase is, therefore, related to the mass density as follows:

$$v''=-\frac{D_{\mathrm{L}}''}{\rho''}\frac{\partial\rho''}{\partial r}.\quad(20)$$

The expression for the function of integration $f'(t)$ for the shell phase, however, is not as obvious as in the previous case. Since the liquid phase volume does not change due to mixing, the rate of change of the droplet volume V, can be expressed as follows:

$$\frac{\mathrm{d}V}{\mathrm{d}t}=4\pi a^{2}\frac{\mathrm{d}a}{\mathrm{d}t}=\frac{1}{\bar{\rho}_{\mathrm{A}}}\frac{\mathrm{d}m_{\mathrm{A}}}{\mathrm{d}t}+\frac{1}{\bar{\rho}_{\mathrm{B}}}\frac{\mathrm{d}m_{\mathrm{B}}}{\mathrm{d}t}.\quad(21)$$

Using Leibnitz's theorem, the rate of change of total mass of A m_{A}, in the droplet can be written as

$$\frac{\mathrm{d}m_{\mathrm{A}}}{\mathrm{d}t}=4\pi\left(\int_{a_{\mathrm{c}}}^{a}\frac{\partial\rho_{\mathrm{A}}'}{\partial t}r^{2}\,\mathrm{d}r+\int_{0}^{a_{\mathrm{c}}}\frac{\partial\rho_{\mathrm{A}}''}{\partial t}r^{2}\,\mathrm{d}r+a^{2}\rho_{\mathrm{As}}'\frac{\mathrm{d}a}{\mathrm{d}t}+a_{\mathrm{c}}^{2}(\rho_{\mathrm{Am}}''-\rho_{\mathrm{Am}}')\frac{\mathrm{d}a_{\mathrm{c}}}{\mathrm{d}t}\right).\quad(22)$$

Replacing the time derivatives in the integrands of equation (22) with the right-hand side of equation (1), integrating the resulting expression, and using equations (4) and (6), we obtain

$$\frac{\mathrm{d}m_{\mathrm{A}}}{\mathrm{d}t}=4\pi r^{2}\left(\rho'D_{\mathrm{L}}'\frac{\partial w_{\mathrm{A}}'}{\partial r}-\rho_{\mathrm{A}}'v'\right)_{r=a}+4\pi a^{2}\rho_{\mathrm{As}}'\frac{\mathrm{d}a}{\mathrm{d}t}\quad(23)$$

which, when combined with equations (18) and (19), yields

$$\frac{\mathrm{d}m_{\mathrm{A}}}{\mathrm{d}t}=\frac{4\pi}{1-b}(\bar{\rho}_{\mathrm{B}}f'(t)-r^{2}\rho'v'|_{r=a})+4\pi a^{2}\rho_{\mathrm{As}}'\frac{\mathrm{d}a}{\mathrm{d}t}.\quad(24)$$

Similarly, we obtain

$$\frac{\mathrm{d}m_{\mathrm{B}}}{\mathrm{d}t}=-\frac{4\pi}{1-b}(\bar{\rho}_{\mathrm{B}}f'(t)-br^{2}\rho'v'|_{r=a})+4\pi a^{2}\rho_{\mathrm{Bs}}'\frac{\mathrm{d}a}{\mathrm{d}t}.\quad(25)$$

Substituting equations (24) and (25) in equation (21), and using the relation in equation (18), we obtain

$$f'(t)=0.\quad(26)$$

The velocity distribution in the shell phase is thus also given by

$$v'=-\frac{D_{\mathrm{L}}'}{\rho'}\frac{\partial\rho'}{\partial r}.\quad(27)$$

Equations (20) and (27) can now be substituted in equation (2), to obtain the following partial differential equation describing the mass concentration distributions in the core and shell phases

$$\frac{\partial\rho^{i}}{\partial t}=\frac{D_{\mathrm{L}}^{i}}{r^{2}}\frac{\partial}{\partial r}\left(r^{2}\frac{\partial\rho^{i}}{\partial r}\right).\quad(28)$$

The complete mathematical description of the problem is now given by the partial differential equations, equations (3) and (28), along with the boundary and initial conditions defined by equations (4) to (12). The following ordinary differential equation obtained from equation (6), using equations (18), (20) and (27), provides the core radius as a function of time,

$$\frac{da_c}{dt} = -\left(\frac{D'_L \frac{\partial \rho'}{\partial r} - D''_L \frac{\partial \rho''}{\partial r}}{\rho' - \rho''}\right)_{r=a_c} \quad (29)$$

with $a_c(0) = a_{ci}$.

The boundary conditions defined by equation (8) are not useful in their present forms. They may, however, be rearranged, using equations (18) and (27), to yield the following boundary condition at the droplet–gas interface ($r = a$):

$$D'_L \frac{\partial \rho'}{\partial r} = \frac{1}{\bar{\rho}_B}\left((\bar{\rho}_B - b\rho')D_A \frac{\partial C_A}{\partial r} + (\bar{\rho}_B - \rho')D_B \frac{\partial C_B}{\partial r}\right)_{r=a} \quad (30)$$

and the ordinary differential equation describing the outer radius as a function of time

$$\frac{da}{dt} = \frac{1}{\bar{\rho}_B}\left(bD_A \frac{\partial C_A}{\partial r} + D_B \frac{\partial C_B}{\partial r}\right)_{r=a} \quad (31)$$

with $a(0) = a_i$. In deriving the above equations, the ratio of the gas phase mass density to the liquid phase mass density has been neglected.

The present problem has two moving boundaries. The model as formulated thus consists of four partial differential equations and two ordinary differential equations that must be solved simultaneously. Boundary conditions given by equations (7) and (30) are non-linear. The problem is thus analytically intractable in the present form. In the present study, we will develop a numerical solution of the system of equations and perform a parametric study to elucidate the effects of various parameters.

3. MODEL IN DIMENSIONLESS FORM

The model as described above is not in a suitable form to be solved by any standard numerical technique. The system involves three spatial domains, the core, shell and gas phases, which are separated by moving boundaries at the core–shell interface $r = a_c(t)$, and the droplet–gas interface $r = a(t)$. The outer boundary of the gas phase is at an infinite distance from the droplet, making the gas phase an ill defined domain for a numerical solution. To circumvent these problems, we introduce the following dimensionless independent variables:

$$X = \frac{r}{a_c(t)}, \quad \text{for } 0 \leqslant r \leqslant a_c(t), \quad (32)$$

$$Y = \frac{a(t) - r}{a(t) - a_c(t)}, \quad \text{for } a_c(t) \leqslant r \leqslant a(t), \quad (33)$$

$$Z = \frac{1}{\sigma}\left(\frac{r}{a(t)} - 1\right), \quad \text{for } a(t) \leqslant r < \infty, \quad (34)$$

$$\tau = \frac{D'_L t}{a_i^2} \quad (35)$$

where σ is a number chosen such that the concentration distributions in the gas phase are not appreciably affected by diffusion at a distance $(\sigma+1)a(t)$ from the droplet center. Transformations given by equations (32) to (34) immobilize the moving boundaries, and scale the spatial domains of all three phases between 0 and 1. The transformation shown in equation (33) was first used by Duda *et al.* [21] for single moving boundary problems, and subsequently, generalized by Saitoh [22]. Avedisian and Suresh [17] applied this transformation to the problem of bubble growth involving two moving boundaries.

The dependent variables are non-dimensionalized by the following transformations:

$$\psi_j = \frac{C_j - C_{j\infty}}{C_{ji} - C_{j\infty}} \quad (36)$$

$$A_c = \frac{a_c(t)}{a_i} \quad (37)$$

$$A = \frac{a(t)}{a_i} \quad (38)$$

where

$$C_{ji} = \frac{P_j^\circ \gamma'_{jm} x'_{jm} M_j}{RT} \quad (39)$$

is the gas phase concentrations at the surface of the droplet at $t = 0^+$.

With the above dimensionless variables, the equations of the model reduce to the following forms:

Core phase

$$\frac{\partial w''_A}{\partial \tau} = \frac{1}{A_c^2}\left[\mathscr{D}_L \frac{\partial^2 w''_A}{\partial X^2} + \frac{\partial w''_A}{\partial X}\left(\frac{2}{X} + \mathscr{D}_L X A_c \frac{dA_c}{d\tau} + \mathscr{D}_L \frac{2(1-b)}{[1-(1-b)w''_A]}\frac{\partial w''_A}{\partial X}\right)\right] \quad (40)$$

with the following initial and boundary conditions:

$$w''_A(X, 0) = w''_{Am} \quad (41)$$

at $X = 0$

$$\frac{\partial w''_A}{\partial X} = 0 \quad (42)$$

at $X = 1$

$$w''_A = w''_{Am}. \quad (43)$$

Shell phase

$$\frac{\partial w'_A}{\partial \tau} = \frac{1}{(A - A_c)^2}\left[\frac{\partial^2 w'_A}{\partial Y^2} + (A - A_c)\frac{\partial w'_A}{\partial Y}\left(-\frac{2}{(1-Y)(A-A_c) + A_c} - Y\frac{dA_c}{d\tau} - (1-Y)\frac{dA}{d\tau}\right) + \frac{2(1-b)}{[1-(1-b)w'_A]}\left(\frac{\partial w'_A}{\partial Y}\right)^2\right] \quad (44)$$

with the following initial and boundary conditions:

$$w'_A(Y,0) = w'_{Am} \tag{45}$$

at $Y = 0$

$$\frac{1}{(A-A_c)}\frac{\partial w'_A}{\partial Y} = \frac{\varepsilon[1-(1-b)w'_A]}{\sigma A} \times \left(\frac{D_B \beta w'_A}{\mu}(\hat{a}'_{Bm} - s_B)\frac{\partial \psi_B}{\partial Z} - \mathscr{D}_A(1-w'_A)(\hat{a}'_{Am} - s_A)\frac{\partial \psi_A}{\partial Z}\right)_{Z=0} \tag{46}$$

at $Y = 1$

$$w'_A = w'_{Am}. \tag{47}$$

Gas phase

$$\frac{\partial \psi_j}{\partial \tau} = \frac{1}{A^2}\left[\frac{D_j}{\sigma^2}\frac{\partial^2 \psi_j}{\partial Z^2} + \frac{\partial \psi_j}{\partial Z}\left(\frac{2D_j}{(1+\sigma Z)\sigma} + \frac{(1+\sigma Z)}{\sigma}A\frac{dA}{d\tau}\right)\right] \tag{48}$$

with the following initial and boundary conditions:

$$\psi_j(Z,0) = 0 \tag{49}$$

at $Z = 0$

$$\psi_j = \frac{\hat{a}'_{js} - s_j}{\hat{a}'_{jm} - s_j} \tag{50}$$

at $Z = 1$

$$\psi_j = 0. \tag{51}$$

Droplet–gas interface

$$\frac{dA}{d\tau} = \frac{\varepsilon}{\sigma A}\left(\frac{D_B \beta}{\mu}(\hat{a}'_{Bm} - s_B)\frac{\partial \psi_B}{\partial Z} + \mathscr{D}_A b(\hat{a}'_{Am} - s_A)\frac{\partial \psi_A}{\partial Z}\right)_{Z=0} \tag{52}$$

with the initial condition

$$A(0) = 1. \tag{53}$$

Core–shell interface

$$\frac{dA_c}{d\tau} = \frac{1}{w'_A - w''_A}\left(\frac{[1-(1-b)w''_A]}{(A-A_c)[1-(1-b)w'_A]}\frac{\partial w'_A}{\partial Y} + \frac{D_L[1-(1-b)w'_A]\partial w''_A}{A_c[1-(1-b)w''_A]\partial X}\right)_{X,Y=1} \tag{54}$$

$$A_c(0) = A_{ci} = \frac{a_{ci}}{a_i}. \tag{55}$$

The parameters in equations (44) to (55) are defined as follows:

$$\beta = \frac{P^s_B}{P^s_A}, \quad \varepsilon = \frac{C_{Ac}}{\bar{\rho}_B}, \quad C_{Ac} = \frac{P^s_A M_A}{RT}, \quad s_j = \frac{C_{j\infty}}{C_{jc}},$$

$$\hat{a}'_j = \gamma'_j x'_j, \quad \mathscr{D}_j = \frac{D_j}{D_L}, \quad \mathscr{D}_L = \frac{D'_L}{D_L} \quad \text{and} \quad \mu = \frac{M_A}{M_B}.$$

It should be noted that the three domains are scaled between 0 and 1, and thus, the problem has been essentially reduced to a single spatial domain ($0 \leqslant X, Y, Z \leqslant 1$). The moving boundaries at the core–shell interface and droplet–gas interface are immobilized in such a way that the ODE, equation (52), describing the outer radius as a function of time is coupled with the PDEs at $Y = Z = 0$, while the ODE, equation (54), describing the core radius is coupled at $X = Y = 1$. Moreover, the PDEs, equations (40), (44) and (48), are coupled by the equilibrium condition, equations (43) and (47), at $X = Y = 1$, and by the boundary condition, equation (46), at $Y = Z = 0$. The resulting system of equations to be solved thus reduces to four PDEs defined in the identical spatial domain between 0 and 1, coupled to two ODEs at $X = 0$ and $X = 1$, respectively. The spatial variables X, Y and Z given above are labeled identically in the computer program, though the distinction is maintained here for clarity.

4. SOLUTION BY NUMERICAL METHODS

The system of differential equations described above is solved by using a numerical software package called SPRINT (Software for Problems in Time). Berzins *et al.* [23, 24] introduced SPRINT for numerical solutions of coupled systems of time-dependent algebraic, ordinary, and partial differential equations. SPRINT uses the Method of Lines (MOL) for solving a system of partial differential equations (PDEs). The space derivatives are discretized over a number of user specified space points NPTS, using either finite difference, finite element or collocation methods resulting in a system of NPTS non-linear, coupled ordinary differential equations (ODEs) for each given PDE. A versatile set of time integrators, based on Gear, theta, variable theta and switching, and blended linear and multi-step methods, are available for solutions of initial value ODEs. The errors associated with the time integration procedure is controllable to a user specified value for the relative error RTOL, and absolute error ATOL, tolerances. SPRINT in its present form can handle a system having a maximum number of 1000 initial value ODEs. Due to this limitation, the number of mesh points NPTS, is restricted by the number of PDEs to be solved.

In the present study SPRITE interface of SPRINT, a finite difference method, is used to solve the system of equations described above. SPRITE is a simplified

interface of SPRINT which provides a calling sequence of SPRINT. The discretization method is based on a lumped finite element method in which a three-point finite difference formula is modified to provide a second-order accuracy. The errors associated with the spatial discretization depend on the number and location of the break-points that define the subintervals. For the present problem, the concentration distributions are expected to have relatively steep gradients near the droplet–gas interface (i.e. near $X = 0$) and near the core–shell interface (i.e. near $X = 1$). Therefore, small subintervals near $X = 0$ and $X = 1$ and larger subintervals in between were used in the present study. For time integration Gear method was chosen. Using a trial and error procedure NPTS = 248, the maximum number of break-points allowable by SPRINT, RTOL = 10^{-3} and ATOL = 10^{-3} were selected.

Since the composition in the shell phase at $t = 0$, is given by the equilibrium relation at the core–shell interface and has a non-zero value, the initial conditions given by equation (49) are inconsistent with the boundary conditions given by equation (50) at $t = 0$. The software package is well suited for the present system because of its ability to handle inconsistent initial and boundary conditions. The software uses a small time step as long as the inconsistencies exist at the boundary.

The value of the parameter σ defining infinity in the gas phase was obtained by a trial and procedure such that the concentration profiles did not alter with higher values. A value of $\sigma = 100$ satisfied the criterion. The accuracy of the numerical method was tested by comparing the results of the present model with the results for a pseudo-steady state model. In the pseudo-steady state model the time derivatives of the partial differential equations of the present transient model were equated to zero. The resulting ordinary differential equations were solved analytically, and the results agreed with that of the present model as long as $\varepsilon\beta < 10^{-7}$. Values of $\varepsilon\beta > 10^{-7}$, imply that the components of the system are relatively volatile, and the core and outer radii change relatively fast. The system is not thus expected to behave in the manner of a pseudo-steady state system.

5. PHYSICAL PARAMETERS

The solution of the model as formulated depends on twelve independent dimensionless parameters: A_{ci}, b, $\mathscr{D}_A$, $\mathscr{D}_B$, $\mathscr{D}_L$, s_A, s_B, x'_{Am}, x''_{Am}, β, ε and μ. Moreover two relations are needed for the activity coefficients of A and B as functions of compositions. In the present study, we shall use the van Laar equations [25]

$$\ln \gamma_A = \frac{A_p}{\left(1 + \frac{A_p x_A}{B_p(1-x_A)}\right)^2} \tag{56}$$

$$\ln \gamma_B = \frac{B_p}{\left(1 + \frac{B_p(1-x_A)}{A_p x_A}\right)^2}. \tag{57}$$

When the miscibility limits, x'_{Bm} and x''_{Am}, are known, the constants A_p and B_p in the above equations can be obtained by satisfying the equilibrium conditions given by equation (5). The relations for the activity coefficients do not thus introduce any more independent dimensionless parameters.

In this study, we shall consider only evaporation in vapor free atmospheres, and thus, the bulk gas saturation ratio parameters assume $s_A = 0$ and $s_B = 0$, values. We shall examine critically the effects of relative volatility β, initial dimensionless core radius A_{ci}, dimensionless saturation concentration of A ε, and relative density b, and present a parametric study by varying each of these parameters one at a time while keeping the rest of the parameters at their default values. Table 1 lists the default values of the parameters used in this study.

Although the model makes no distinction between components A and B, we have taken the core phase to be enriched with component B while the shell phase with component A. The problem, however, can also be solved by reversing the components of the core and the shell phases.

6. RESULTS AND DISCUSSION

For the present problem, the core and shell radii continuously change with time and the system is in a transient state at all times. The gas and droplet phase concentration distributions also change with time as long as the evaporation process continues. The initial and boundary conditions for the core phase are, however, such that the core phase composition distribution remains at the initial value of $x''_A = x''_{Am}$, for $0 \leqslant r \leqslant a_c$, at all times. The gas and shell phase composition distributions as functions of time depend on the physical properties and the dimensions of the

Table 1. Default values of dimensionless parameters used in this study

Parameter	Default value
A_{ci}	0.80
b	0.50
$\mathscr{D}_A$	10^5
$\mathscr{D}_B$	5.0×10^4
$\mathscr{D}_L$	1.0
s_A	0
s_B	0
x'_{Am}	0.98
x''_{Am}	0.10
A_p	2.6238
B_p	4.0709
β	1
ε	10^{-7}
μ	0.50
σ	100

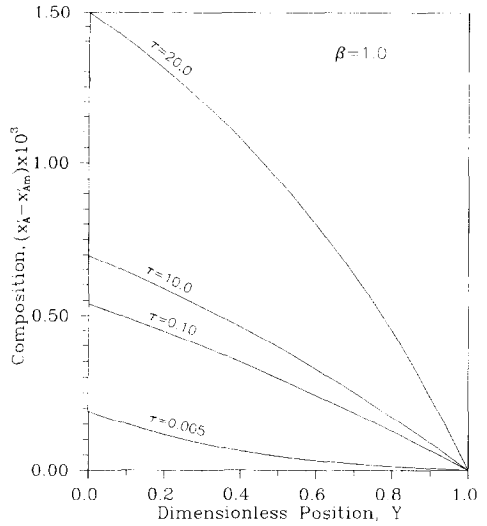

FIG. 2. Shell phase composition distribution at various times for $\beta = 1.0$.

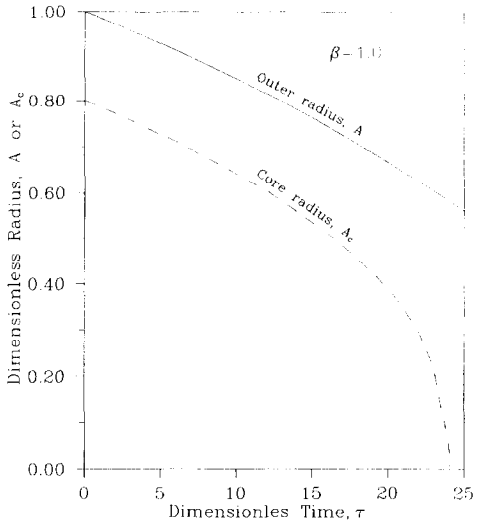

FIG. 4. Core and outer radii as functions of time for $\beta = 1.0$.

droplet. For the parameter values listed in Table 1, Figs. 2–4 show concentration profiles in the shell and gas phases at various times, and the outer and core radii as functions of time, respectively.

Figure 2 shows that the composition at the core–shell interface (i.e. $Y = 1$) always remains at $x'_A = x'_{Am}$, as specified by the equilibrium boundary condition. At all times, the mole fraction of x'_A, as a function of position decreases from the value x'_{As}, at the droplet–gas interface to the equilibrium value x'_{Am}, at the core–shell interface. The composition at the droplet–gas interface continuously increases above the initial value x'_{Am}, as time progresses. The shell phase composition distribution as a function of time depends on the relative evaporation rates of components A and B. For the surface composition x'_{As}, to increase initially, the ratio of the initial evaporation rate of B to that of A must exceed the initial composition ratio of B to A in the shell phase. This condition can be expressed mathematically as follows:

$$\left.\frac{dx'_{As}}{d\tau}\right|_{\tau=0} > 0, \quad \text{if } \beta \frac{D_B \gamma'_{Bm} x'_{Bm}}{D_A \gamma'_{Am} x'_{Am}} > \frac{x'_{Bm}}{x'_{Am}}. \tag{58}$$

where the left-hand side term of the second inequality represents the ratio of the initial evaporation rates. For the values listed in Table 1, the condition in equation (58) is satisfied. The initial increase in the surface composition of A can thus be explained. When the ratio of the evaporation rate of B to that of A exceeds the composition ratio of B to A in the shell phase, the core phase shrinks by supplying to the shell phase the excess amount of B lost by evaporation. Figure 4 shows that the core radius indeed decreases as a function of time.

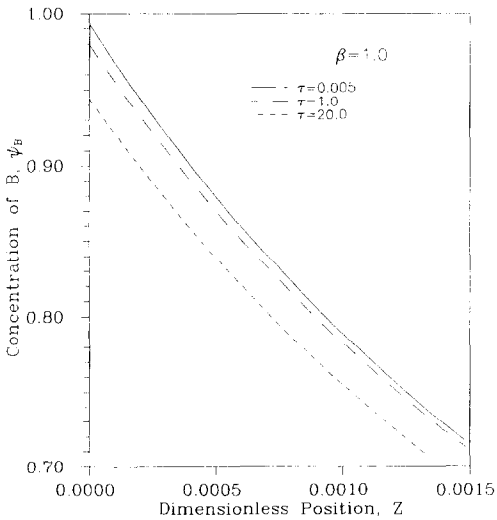

FIG. 3. Gas phase concentration distribution at various times for $\beta = 1.0$.

The gas and shell phase concentration distributions as functions of time have two distinct periods: a short transient period followed by a long dynamic steady period. During the initial transient period, the concentration distributions develop in the gas and shell phases, and change rapidly to dynamic steady state values. During the dynamic steady state period, the gas and liquid phase transfer rates, and the outer and core radii change relatively slowly. The change of interfacial composition during this period depends on the gas and shell phase interfacial transfer rates, and the rate of change of the outer radius, as indicated by the boundary conditions given by equation (8). For the case in Fig. 2, x'_{As} continuously increases as time progresses. To examine the gas phase transfer, in Fig. 3, we have plotted the dimensionless gas phase concentration as a function of position for various values of τ. The gas phase concentration decreases from the surface value at $Z = 0$ to the bulk value $\psi_B = 0$ at $Z = 1$. The droplet surface concentration follows the equilibrium relation given by equation (7), and decreases as the surface composition of B x'_{Bs}, in the shell phase decreases as time progresses. The inter-

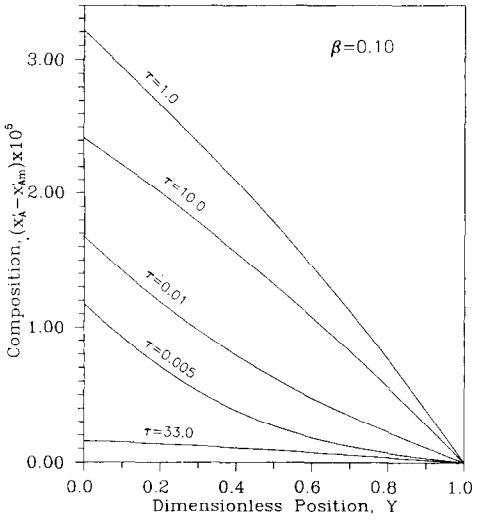

FIG. 5. Shell phase composition distribution at various times for $\beta = 0.10$.

facial gas phase diffusional transfer rate thus follows the interfacial composition trend, and for the present case it decreases for component B. The balance of equation (8) is thus dictated by the shell phase transfer rate. The transfer rate of a component from the core–shell interface to the droplet–gas interface depends on the shell thickness $(A - A_c)$. Figure 4 shows that the outer and core radii decrease with time but the core radius decreases faster than the outer radius. The shell thickness $(A - A_c)$ thus increases as time progresses. Finally the core disappears completely at $\tau = 24$, leaving a single-phase droplet of final size $A = 0.585$. The increasing shell thickness reduces the transfer rate of component B from the core–shell interface to the droplet–gas interface, and to maintain the balance of equation (8), the surface composition x'_{Bs} (or x'_{As}) decreases (or increases) with time as shown in Fig. 2.

The concentration distributions and the dimensions of a layered droplet as functions of time depends on the physical properties of the system. Figures 5 and 6 show the shell phase composition distribution and the outer and core radii as functions of time, respectively, for $\beta = 0.10$. The value of β can be decreased by lowering the vapor pressure of component B P°_B, when the other physical properties are kept at the same values. The condition in equation (58) is satisfied for $\beta = 0.10$. Figure 5 shows that the droplet surface composition x'_{As}, rapidly increases to a maximum value during the initial transient period, and then slowly decreases with time. For this case, Fig. 6 shows that both the outer and the core radii decrease with time but the outer radius decreases faster than the core radius. The shell thickness thus decreases as time progresses. Finally the shell evaporates completely at $\tau = 34$, leaving a single phase droplet of final size $A = A_c = 0.777$. The decrease of the surface composition during the dynamic steady period is due to the decreasing shell thickness.

The physical process reverses when the value of β decreases to 0.01. Figures 7 and 8 show the shell phase composition distribution and the outer and core radii as functions of time, respectively, for $\beta = 0.01$. For this case, the ratio of the initial evaporation rate of A to that of B exceeds the initial composition ratio of A to B in the shell phase. Figure 7 shows the surface composition decreases rapidly to a minimum value from the initial value x'_{Am}, during the transient period, and then the surface composition increases slowly. At all times, the composition of B everywhere in the shell phase exceeds the miscibility limit x'_{Bm} (i.e. $x'_A \leqslant x'_{Am}$), and it decreases from the surface value to the miscibility limit value x'_{Bm}, at the core–shell interface. In addition to the shrinkage due to the evaporation, the shell phase thus also shrinks by supplying a proportionate amount of A and B to the core phase, and the core phase grows. Figure 8 shows that the outer radius decreases while core radius increases. At $\tau = 34$, the shell collapses on the core, and during this period the core grows from the initial value of

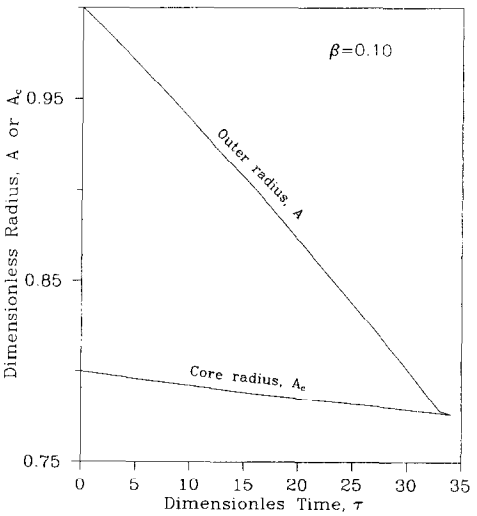

FIG. 6. Core and outer radii as functions of time for $\beta = 0.10$.

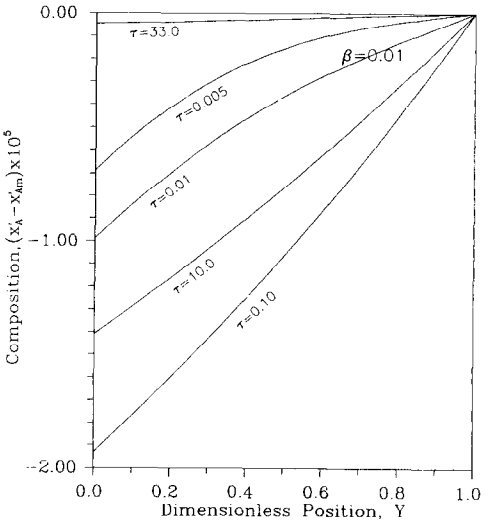

FIG. 7. Shell phase composition distribution at various times for $\beta = 0.01$.

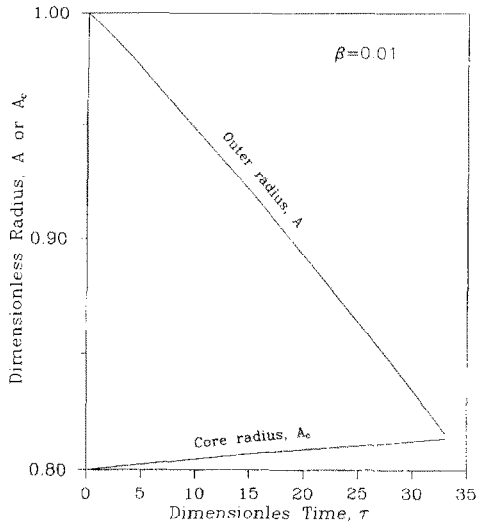

FIG. 8. Core and outer radii as functions of time for $\beta = 0.01$.

$A_{ci} = 0.80$ to a final value $A = A_c = 0.813$. Since the shell thickness continually decreases, the surface composition x_{As}, increases after attaining a minimum value at the end of the transient period. At $\tau = 33$, when the shell is very thin, Fig. 7 shows the composition distribution becomes almost uniform with a value of $x'_A = x'_{Am}$.

The preceding examples show that depending on the value of β, the core either evaporates or grows during the evaporation of a layered droplet, eventually forming a single-phase droplet enriched with either component A or component B. When the core evaporates, the core eventually disappears for $\beta = 1.0$, and the shell collapses on the core for $\beta = 0.10$. For a given droplet dimension the relative volatilities of components A and B dictate the final composition of the single-phase droplet. Similarly, for a given set of physical properties, the composition of the final single-phase droplet is dictated by the initial dimensions. Table 2 shows the effect of the initial value of the dimensionless core radius. As the initial core radius increases, the time required for the formation of a single-phase droplet increases when the core disappears. For $A_{ci} \leqslant 0.8$, the core disappears completely, and for $A_{ci} = 0.9$, the shell evaporates completely. The results indicate that there is a critical initial core radius, between 0.80 and 0.90, for which both the core and shell disappear simultaneously. This critical value depends on the physical properties of the system.

Table 2. Effect of initial shell thickness

Initial core radius, A_{ci}	Final time τ	Final core radius, A_c	Final outer radius, A
0.50	6.33	0.000	0.916
0.60	10.0	0.000	0.860
0.70	15.5	0.000	0.766
0.80	24.0	0.000	0.585
0.90	20.0	0.655	0.655

Table 3. Effect of volatility parameter ε

Volatility parameter ε	Final time τ	Final core radius, A_c	Final outer radius, A
1×10^{-9}	2.23×10^{3}	0.000	0.587
1×10^{-8}	2.31×10^{2}	0.000	0.586
1×10^{-7}	2.35×10^{1}	0.000	0.582
1×10^{-6}	3.49×10^{0}	0.000	0.445
1×10^{-5}	3.80×10^{-1}	0.552	0.552

The effect of the volatility parameter ε, is shown in Table 3. When all the other parameters remain at the same values, a change in the volatility parameter by a factor represents changes of the vapor pressures of A and B by the same factor. As the volatility parameter increases, Table 3 shows that the duration of persistence of a layered droplet as a two phase droplet shortens. For $\varepsilon < 10^{-6}$, the core disappears completely, and for $\varepsilon = 10^{-5}$, the shell evaporates completely. For low values of ε (i.e. $\leqslant 10^{-7}$), the size of the final single phase droplet is independent of ε, and the time required for its formation is almost inversely proportional to the value of ε.

The densities of the components can also significantly affect the evaporation process of a layered droplet. Table 4 shows the effect of the relative density parameter b. A change of b alone represents a change of the density of component A, $\bar{\rho}_A$. For $b < 0.9$, the core disappears and for $b \geqslant 0.90$, the shell disappears. When the core disappears, an increase of b or a reduction of the density of component A, decreases the final single-phase droplet size and increases the time required for its formation. When the shell disappears, an increase of b increases the final single-phase droplet size and reduces the time required for its formation. The densities affect the evaporation rates two ways: by altering the volume change for a given mass change due to the evaporation, and by altering the magnitude and direction of the convective velocity generated by the density difference. Since the composition of A decreases from the droplet surface to the core–shell interface for an evaporating core, equation (27) shows that the convective velocity is directed towards the core for $b < 1$, and towards the droplet surface for $b > 1$. The core evaporation rate is then retarded for $b < 1$, and is enhanced for $b > 1$,

Table 4. Effect of relative density parameter b

Relative density parameter, b	Final time τ	Final core radius, A_c	Final outer radius, A
0.50	24.0	0.000	0.585
0.70	25.7	0.000	0.417
0.80	26.9	0.000	0.300
0.90	25.0	0.313	0.313
1.10	20.0	0.470	0.470
1.30	15.5	0.550	0.550
1.50	14.0	0.587	0.587

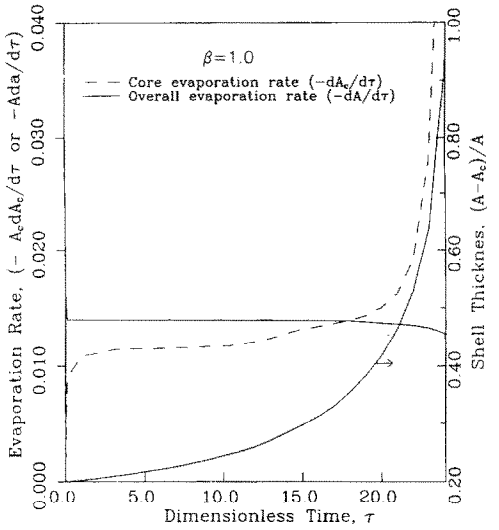

FIG. 9. Overall and core evaporation rates, and shell thickness as functions of time.

by the convective transport. An increase of b or a reduction of the density of component A, increases the evaporation of the shell, and consequently, the reduction of the shell thickness increases the evaporation rate of the core. The combination of these two effects then dictates the final fate of a layered droplet.

Another interesting aspect associated with the evaporation of a layered droplet is the evaporation rates of the core and shell phases. In a recent experimental study, Ray *et al.* [19] observed that the evaporation rate of a core glycerol droplet coated with non-volatile dioctyl phthalate increases as the layer thickness increases. To examine this phenomena, we have plotted instantaneous evaporation rates of core and shell phases, $-A_c\,dA_c/d\tau$ and $-A\,dA/d\tau$, and the shell thickness as functions of time in Fig. 9 for $\beta = 1$. For this situation the shell thickness, defined by

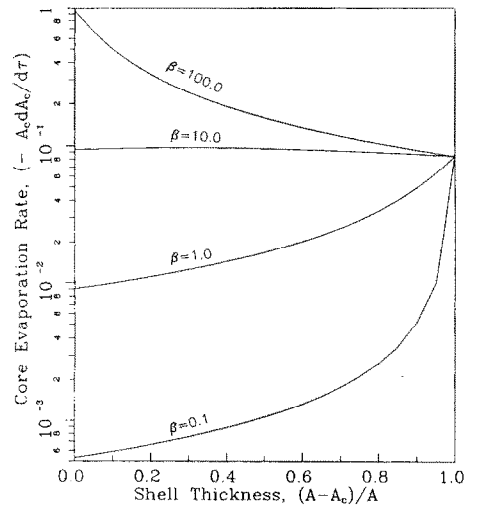

FIG. 10. Core evaporation rate as a function of shell thickness for various values of β.

$(A-A_c)/A$, increases continuously, and the core eventually disappears. The results show that the overall evaporation rate $(-A\,dA/d\tau)$ remains nearly the same for all values of time, except during the initial transient period and when the core disappears. Thus, the overall evaporation behavior can approximately be described by a linear relation between A^2 and τ. The core evaporation rate $(-A_c\,dA_c/d\tau)$, however, continuously increases with time, and follows the trend of the shell thickness, that is, the core evaporation rate increases as the shell thickness increases with time. This behavior is similar to the observation of Ray *et al.* [19].

To examine the relation between the shell thickness and core evaporation rate, we have plotted the instantaneous core evaporation rate after the initial transient period as a function of the shell thickness for various values of β. The results show that for $\beta \leqslant 10$, the core evaporation rate increases and for $\beta > 10$, core evaporation rate decreases as the shell thickness increases. This behavior can be understood qualitatively by considering two competing effects. For a given core radius, as the shell thickness increases the outer surface area available for evaporation of molecules enriching the core phase increases. As the shell thickness increases, the diffusional resistance, however, lowers the composition of B (i.e. the component enriching the core) at the outer surface as can be seen from Figs. 2 and 4. The former effect enhances while the latter effect retards the core evaporation rate. Whether the combined effect of these two opposing tendencies increases or decreases the core evaporation rate depends on the physical properties of the system.

7. CONCLUSIONS

We have developed a mathematical model for the evaporation and growth of a layered droplet of two partially miscible components exposed to a stagnant gas phase. The model equations describe the unsteady state transport of two components in the gas, shell and core phases, and the outer and core radii as functions of time. The model shows that the evaporation and growth processes depend on twelve dimensionless parameters. We have solved the model equations, using a numerical technique, and presented results showing the effects of various parameters on the evaporation and growth dynamics of a layered droplet. In a vapor-free atmosphere where both components of the droplet evaporate, the results show that the core may evaporate or grow depending on the physical properties of the system. At the gas–droplet interface, the composition of the component enriching the core phase always remains above the miscibility limit for a growing core and below the miscibility limit for an evaporating core; however, depending on the shell thickness, the interfacial composition may increase, decrease or show a maximum or a minimum as a function of time. The analysis suggests that the process of evaporation and growth has two distinct

periods: an initial short transient period followed by a long dynamic steady period. During the transient period, the concentrations in the shell and gas phases rapidly develop to dynamic steady levels. For an evaporating core, during the dynamic steady period, the composition of the core enriching component at the outer surface decreases as the shell thickness increases. For a given core droplet, however, as the shell thickness increases, the outer surface area available for the evaporation of the component increases. As a consequence, the core evaporation rate may increase or decrease with increasing shell thickness, depending on the relative magnitudes of these two opposing effects on the evaporation of the component enriching the core. When the core evaporates, depending on the initial dimensions of the droplet, either the core or the shell eventualy disappears, leaving a single phase droplet enriched with one of the components. At a critical initial core radius, whose value depends on the physical properties, the core and shell phases disappear simultaneously.

Acknowledgements—We are grateful to the National Science Foundation (Grant No. CTS-8912282), U.S. Army Chemical RD&E Center (Battelle Contract # DAAL03-86-D-001) and Brown and Williamson Tobacco Corp. for their generous support.

REFERENCES

1. N. A. Fuchs, *Evaporation and Droplet Growth in Gaseous Media*. Pergamon, New York (1959).
2. G. O. Rubel, On the evaporation rates of multicomponent oil droplets, *J. Colloid Interface Sci.* **81**, 188–195 (1981).
3. C. B. Richardson, H. B. Lin, R. McGraw and I. N. Tang, Growth rate measurements for single suspended droplets using the optical resonance method, *Aerosol Sci. Technol.* **5**, 103 (1986).
4. G. Sageev, R. C. Flagan, J. H. Seinfeld and S. Arnold, Condensation rate of water on aqueous droplets, *J. Colloid Interface Sci.* **113**, 421 (1987).
5. A. K. Ray, R. D. Johnson and A. Souyri, Dynamic behavior of single glycerol droplets in humid air streams, *Langmuir* **5**, 133–140 (1989).
6. J. L. Huckaby and A. K. Ray, Absorption of sulphur dioxide by growing and evaporating water droplets, *Chem. Engng Sci.* **44**, 2797–2808 (1989).
7. C. K. Law, C. H. Lee and N. Srinivasan, Combustion characteristics of water-in-oil emulsion droplets, *Combustion Flame* **37**, 125–143 (1980).
8. C. T. Avedisian and M. Fatehi, An experimental study of the Leidenfrost evaporation characteristics of emulsified liquid droplets, *Int. J. Heat Mass Transfer* **31**, 1587–1603 (1988).
9. V. K. La Mer, *Retardation of Evaporation by Monolayers*. Academic, New York (1962).
10. D. C. Taflin, S. H. Zhang, T. Allen and E. J. Davis, Measurement of droplet interfacial phenomena by light scattering techniques, *A.I.Ch.E. Jl* **34**, 8 (1988).
11. G. O. Rubel and J. W. Gentry, Measurements of the kinetics of solution droplets in the presence of absorbed monolayers: determination of water accommodation coefficients, *J. Phys. Chem.* **88**, 3142–3148 (1984).
12. G. O. Rubel and J. W. Gentry, Measurement of water accommodation coefficients at surfaces covered with adsorbed monolayers of hexadecanol, *J. Aerosol Sci.* **16**, 571 (1985).
13. T. I. Quickenden and G. T. Barnes, Evaporation through monolayers—theoretical treatment of the effect of chain length, *J. Colloid Interface Sci.* **67**, 415 (1978).
14. R. E. Plevan and J. A. Quinn, The effect of monomolecular films on the rate of gas absorption into a quiescent liquid, *A.I.Ch.E. Jl* **12**, 894 (1966).
15. T. G. Springer and R. L. Pigford, Influence of surface turbulence and surfactants on gas transport through liquid interfaces, *Ind. Engng Chem. Fundam.* **9**, 458 (1970).
16. D. D. Frey and C. J. King, Effects of surfactants on mass transfer during spray drying, *A.I.Ch.E. Jl* **32**, 437 (1986).
17. C. T. Avedisian and K. Suresh, Analysis of non-explosive bubble growth within a superheated liquid droplet suspended in an immiscible liquid, *Chem. Engng Sci.* **40**, 2249–2259 (1985).
18. D. W. Readey and A. R. Cooper, Molecular diffusion with a moving boundary and a spherical symmetry, *Chem. Engng Sci.* **21**, 917–922 (1966).
19. A. K. Ray, B. Devakottai, A. Souyri and J. L. Huckaby, Evaporation characteristics of droplets coated with immiscible layers of nonvolatile liquids, *Langmuir* **7**, 525–531 (1991).
20. D. E. Rosner and W. S. Chang, Transient evaporation and combustion of a fuel droplet near its critical point, *Combust. Sci. Technol.* **7**, 145–158 (1973).
21. J. L. Duda, M. F. Malone and R. H. Notter, Analysis of two-dimensional diffusion-controlled moving boundary problems, *Int. J. Heat Mass Transfer* **18**, 901–910 (1975).
22. T. Saitoh, Numerical method for multi-dimensional freezing problems in arbitrary domains, *J. Heat Transfer* **100**, 294–299 (1978).
23. M. Berzins, P. M. Dew and R. M. Furzeland, *Software for Time-dependent Problems in PDE Software Modules, Interfaces and Systems* (Edited by B. Engquist and T. Smedsaas). North Holland, Amsterdam (1984).
24. M. Berzins and R. M. Furzeland, A user's manual for SPRINT—a versatile software package for solving systems of algebraic, ordinary and partial differential equations: Part 2—partial differential equations, TNER.86.050, Thornton Research Center, Shell Research Ltd., Chester, England (1989).
25. S. M. Waals, *Phase Equilibria in Chemical Engineering*. Butterworths, Boston (1985).

DYNAMIQUE DE CROISSANCE DE L'EVAPORATION D'UNE GOUTTELETTE STRATIFIEE

Résumé—Un modèle mathématique est formulé pour l'évaporation croissante d'une gouttelette unique, diphasique, à deux composants partiellement miscibles, exposée à une phase gazeuse au repos. On traite rigoureusement les équations de transport instationnaire des deux composants dans les phases du coeur, de la peau et du gaz. Le modèle mathématique impliquant deux limites mobiles à l'interface coeur–peau et à l'interface gouttelette–gaz a été résolu numériquement pour différentes conditions. On examine les effets des paramètres critiques sur la dynamique des gouttelettes. Quand les deux composants s'évaporent dans l'atmosphère, le coeur croît ou s'évapore selon les paramètres physiques. Quand le coeur s'évapore, soit la peau soit le coeur disparaît en premier, laissant une goutte à une seule phase. L'étude montre que la volatilité des composants, les paramètres thermodynamiques et de transport influencent fortement l'évaporation d'une gouttelette stratifiée.

VERDAMPFUNGS- UND WACHSTUMSVERHALTEN EINES GESCHICHTETEN TROPFENS

Zusammenfassung—Für Verdampfung und Wachstum eines zweiphasigen isolierten Tropfens, der aus zwei teilweise mischbaren Komponenten besteht, wird ein mathematisches Modell aufgestellt. Der Tropfen befindet sich in einer ruhenden Gasphase. Für die beiden Komponenten im Kern, in der Hülle und in der Gasphase werden die instationären Transportgleichungen exakt formuliert. Das sich ergebende mathematische Modell schließt die beiden beweglichen Phasengrenzen zwischen Kern und Hülle einerseits sowie Tropfen und Gas andererseits ein. Die numerische Lösung erfolgt für verschiedene Bedingungen. Die kritischen Einflußparameter für das Verhalten des Tropfens werden untersucht. In einer dampffreien Umgebung verdampfen beide Komponenten, wobei der Kern abhängig von den physikalischen Parametern entweder anwächst oder verdampft. Im Fall der Verdampfung das Kerns verschwindet als erstes die Hülle oder der Kern, so daß ein einphasiger Tropfen zurückbleibt. Die Untersuchung zeigt, daß die Flüssigkeit der Komponenten sowie die thermodynamischen und die Transportparamter das Verdampfungsverhalten eines geschichteten Tropfens sehr stark beeinflussen.

ИСПАРЕНИЕ И ДИНАМИКА РОСТА СЛОИСТОЙ КАПЛИ

Аннотация—Сформулирована математическая модель испарения и роста двухфазной изолированой капли, состоящей из двух частично смешивающихся компонентов, при воздействии неподвижной газовой фазы. Детально рассматриваются нестационарные уравнения переноса для обоих компонентов в ядре, оболочке и газовой фазе. Численно решается результирующая математическая модель, включающая две движущиеся границы на поверхностях раздела ядро–оболочка и капля–газ в различных условиях. Исследуется влияние критических параметров на динамику капель. При испарении обоих компонентов в атмосфере, не содержащей пара, результаты показывают, что ядро растет или испаряется в зависимости от физических параметров. При испарении ядра исчезает оболочка или ядро, после чего остается однофазная капля. Показано, что летучесть компонянтов, а также термодинамические характеристики и параметры переноса оказывают сильное влияние на процесс испарения слоистой капли.